TISSUE ENGINEERING: Part A
Volume 19, Numbers 21 and 22, 2013

DOI: 10.1089/ten.tea.2012.0733

Brain Tissue Interaction with Three-Dimensional, Honeycomb Polycaprolactone-Based Scaffolds Designed for Cranial Reconstruction Following Traumatic Brain Injury

David Kim Seng Choy, MBBS, FRCS (Neurosurgery),[1] Vincent Diong Weng Nga, MBBS, MRCS (Edinburgh),[1] Jing Lim, MEng,[2] Jia Lu, MD, PhD,[3,4] Ning Chou, MBBCh, FRCSEd (Gen Surg),[1] Tseng Tsai Yeo, MBBS, FRACS (Neurosurgery),[1] and Swee-Hin Teoh, PhD[2]

Following traumatic brain injury (TBI), resultant voids are unable to support injections of suspension treatments, leading to ineffective healing. Moreover, without a structure to support the large defect, the defect site suffers from mechanical instability, which may impair the healing process. Therefore, having a delivery vehicle that can temporarily fill and provide mechanical support to the defect site may alleviate the healing process. In this work, we reported for the first time, the inflammatory response of brain tissue with polycaprolactone (PCL) and PCL-tricalcium phosphate (TCP) scaffolds designed and fabricated for cranial reconstruction. After cranial defects were created in Sprague-Dawley rats, PCL and PCL-TCP scaffolds were implanted for a period of 1 week and 1 month. Following histology and immunofluorescence staining with the ionized calcium binding adaptor molecule-1 (*IBA-1*), glial fibrillary acidic protein (*GFAP*), nestin, and neuronal nuclei (*NeuN*), results indicated that *IBA-1*-positive activated microglia were observed across all groups, and declined significantly by 1 month ($p < 0.05$). Interestingly, *IBA-1*-positive microglia were significantly fewer in the PCL-TCP group ($p < 0.05$), suggesting a relatively milder inflammatory response. A decrease in the number of *GFAP*-positive cells among all groups over time (>29%) was also observed. Initially, astrocyte hypertrophy was observed proximal to the TBI site (55% in PCL and PCL-TCP groups, 75% in control groups), but it subsided by 1 month. Proximal to the TBI site, nestin immunoreactivity was intense during week 1, and which reduced by 1 month across all groups. *NeuN*-positive neurons were shrunken proximal to the TBI site (<0.9 mm), 32% smaller in the PCL-TCP group and 27% smaller in the PCL group. Based on above data indicating the comparatively milder, initial inflammatory response of brain tissue to PCL-TCP scaffolds, it is suggested that PCL-TCP scaffolds have notable clinical advantages as compared to PCL scaffolds.

Introduction

Following traumatic brain injury (TBI), complex biochemical and molecular cascades may lead to neurological complications. Direct injections of pharmaceutical agents such as cells[1,2] and growth factors[3–5] may diffuse from the site of insult to surrounding tissue, greatly affecting the effectiveness of this technique.[6] Tissue engineering (TE) may be able to provide an alternative to enhancing current treatment methods, by using a tissue-engineered cranial scaffold to contain pharmaceutical agents, cells, and growth factors for efficient delivery.[7,8] A suitable delivery vehicle for cranial TE should allow for tissue ingrowth from host, immunological compatibility, biocompatibility, suitable degradation characteristics, and by-products to avoid undesirable inflammatory responses that further worsen injury.[6] The combination of suitable materials and biological agents may provide an alternative route to successful regeneration of the injured parenchyma.

In this light, a variety of materials have been investigated as delivery vehicles for TBI. Tate *et al.* developed synthetic methylcellulose (MC)-based gel constructs with pore sizes in the range of 30–50 μm, as a biocompatible injectable scaffold.[9] Polymer stability in *in vitro* studies over a 2-week period encouraged their use for TE applications, while MC was recently shown to promote peripheral nerve regeneration.[10] Tian *et al.* prepared a freeze-dried hyaluronic acid and polylysine hydrogel, and investigated its biocompatibility in

[1]Division of Neurosurgery, National University Hospital Singapore, Singapore, Singapore.
[2]Division of Bioengineering, School of Chemical and Biomedical Engineering, Nanyang Technological University, Singapore, Singapore.
[3]Department of Anatomy, Yong Loo Lin School of Medicine, National University of Singapore, Singapore, Singapore.
[4]DSO National Laboratories (DMERI@DSO), Defence Medical and Environmental Research Institute, Singapore, Singapore.

adult rats.[11] Hyaluronic was chosen due to its presence in the natural extracellular matrix (ECM) of the brain, and due to its critical role during brain formation. Infiltration of glial fibrillary acidic protein (*GFAP*)-positive astrocytes and contiguity between a hydrogel and host tissue indicated its biocompatibility. Yasuda *et al.* used a fibrin scaffold for the transplantation of bone marrow stromal cells in rat cortical injury[12] due to its biocompatibility, biodegradability, and ability to adhere to brain tissue. Recently, Wong *et al.* has reported positive effects of using polycaprolactone (PCL) sponges in regeneration following TBI.[6] As aforementioned, the desirable properties of scaffolds have, in one way or the other, been considered in the chosen materials.

Over the years, our group has developed PCL and PCL-tricalcium phosphate (PCL-TCP) as viable biomaterials for TE applications, including skin,[13] bone,[14–16] and drug delivery.[17,18] By using a solvent-free approach of fused deposition modeling, PCL-based scaffolds have been fabricated with a variety of porosities ranging from 70%–90%.[19,20] Morphological observations under a scanning electron microscope revealed an interconnected microarchitecture that has been shown to be a conducive environment for the infiltration, retention, proliferation, and differentiation of cells.[21,22] In treating a large cranial defect, the scaffold support with geometrical integrity may hold advantages over hydrogels by providing sturdier architecture for efficient cells, growth factor, and drug delivery. The degradation profile of PCL and PCL-TCP scaffolds has already been well-characterized by our group both *in vitro* and *in vivo*.[23] Of particular interest would be the ability of PCL-TCP scaffolds to maintain pore interconnectivity despite having a higher degradation rate as compared to PCL, which is conducive for the promotion of vascular infiltration, subsequently initiating a cascade of molecular events to promote tissue ingrowth. At this present moment, the authors note that PCL-TCP scaffolds have not been characterized for brain tissue biocompatibility in terms of its inflammatory response; therefore, this work has sought to investigate the immunological response of brain tissue in contact with PCL-TCP scaffolds by comparing against control (no implantation) and PCL scaffolds of similar geometry and porosity.

Materials and Methods

Surgical procedure

The animal studies reported in this work have been approved by the animal ethics committee, Institutional Animal Care and Use Committee (IACUC, protocol: IACUC 096/11) at the National University of Singapore. Female Sprague-Dawley rats weighing ~250 g were anesthetized with isofluorane, and their skulls were surgically exposed. The bregma was located, and three positions were marked: 3 mm anterior and 3.5 mm left and right. Holes were drilled at the three locations with a 3-mm outer-diameter trephine (Fig. 1). Bone chips were removed, and 3-mm-deep holes were drilled into the cerebral cortex using the same trephine. The drill was held in position and maintained perpendicular to the surface of the skull.

PCL and PCL-TCP scaffolds (Osteopore International Pte Ltd.) were fabricated using a solvent-free approach of fused deposition modeling,[20,21] to achieve a lay-down pattern of 0°/60°/120° with a porosity of 70%, as reported earlier.[24] To

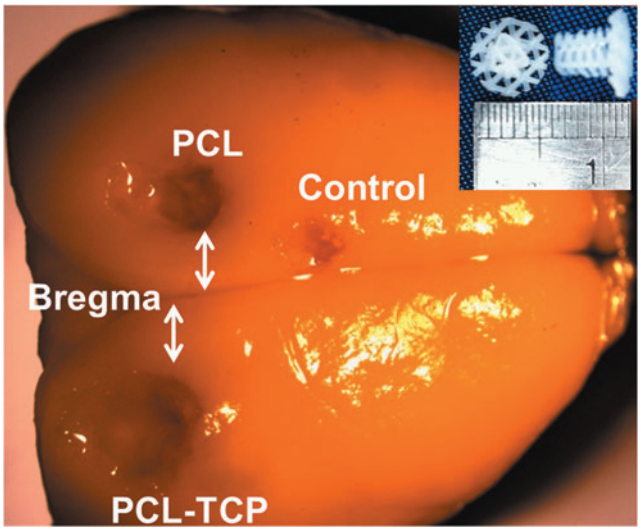

FIG. 1. Representative image of a harvested Sprague-Dawley rat brain, with the bregma, and locations of the scaffolds and controls clearly shown. The scaffolds used were of 3-mm diameter and 3-mm height (inset). PCL, polycaprolactone. Color images available online at www.liebertpub.com/tea

fit the defects created in the rat cranium, the scaffolds were designed in a plug-like manner, as depicted in (Fig. 1, inset). PCL plugs with a diameter of 3 mm were fitted snugly into the cavity left of the bregma, while PCL-TCP scaffolds of similar geometry were fitted snugly into the cavity right of the bregma. Control (3 mm anterior) was left without scaffold implantation.

Two time points were investigated: 1 week and 1 month. At each time point, five rats were sacrificed, their brains harvested and cryoprotected in 30% sucrose, embedded in Tissue-Tek Optimal Cutting Temperature compound (Electron Microscopy Sciences), and then serially sectioned in the coronal plane at 14-mm thickness intervals for further analysis.

Histopathology

Following perfusion, the brains were harvested and postfixed in 10% buffered formalin. The brains were then dehydrated in an ascending series of alcohol, cleared with xylene, and then embedded in paraffin wax. Paraffin sections of 4-m thickness were then cut and microwaved in a citrate buffer for antigen retrieval and blocked with the peroxidise blocking reagent (*S2023*; Dako UK Ltd.). For general histopathology, sections were stained in hematoxylin and eosin (H&E). For immunohistochemistry, sections were incubated with mouse monoclonal anti-neuronal nuclei (*NeuN*) (*MAB377*; Chemicon International, Inc.) diluted 1:600 in phosphate-buffered saline (PBS); mouse monoclonal anti-*GFAP* (*MAB360*; Chemicon International, Inc.) diluted 1:1800 in PBS; rabbit polyclonal anti-ionized calcium binding adaptor molecule *(IBA-1)* (019-19741; Wako Pure Chemical Industries) diluted 1:500 in PBS; mouse monoclonal anti-nestin (*MAB353*; Chemicon International, Inc.) diluted 1:500 in PBS; for detection of *NeuN*, *GFAP*, *IBA-1*, and nestin, respectively. Subsequent antibody detection was carried out using either anti-mouse (rat absorbed) or anti-rabbit *IgG* (ImPRESS Ig reagent kit; Vector Laboratories). All samples

were then visualized using 3,3′-diaminobenzidine and digitalized using Leica SCN400 Automatic Slide scanner and corresponding Image Viewer Software (Leica Microsystems CMS GmbH). All images were taken in one sitting, using the exact same exposure and processing parameters. Baseline readings were taken at regions far from the defect site (>5 mm), with the assumption that at those regions, there is minimal elevation of *GFAP*- or *IBA-1*-positive cells.

Determination of pixel area

Pixel areas for *GFAP* and *IBA-1* were calculated using ImageJ (version 1.46r, National Institute of Health, from http://imagej.nih.gov/ij). Thresholding of the colored images was done, to highlight the regions of interest in black. Following that, images were converted into 8-bit images and then into binary images. Noise was removed by removing outliers, and the binary image was compared to the original image carefully to ensure a good representation of the original. Cell counting and area measurement was then conducted on the processed images. At least three regions were chosen for analysis for each image. A total of four images per anatomical location were used in the calculation of the pixel area. In this study, the proximal region is defined as the region within 0.9 mm of the defect, while the distal region is defined as the region more than 1 mm away from the defect.

To determine statistical significance, the two-tailed Student's *t*-test was conducted, and *p*-values less than 0.05 were considered statistically significant.

Results

Gross observations

Postoperatively, the rats were monitored for any significant weight loss, signs of pain, and severe brain injury. Subcutaneous caprofen and oral neomycin were given for 3 and 7 days, respectively, based on the rats' body weight. There were no deaths postoperative, and the rats recovered spontaneous locomotion within 15 min postoperatively. The rats were inspected daily for the first 7 days and then on a weekly basis. The area of the TBI sites were not measured due to the geometrical and physical properties of PCL and PCL-TCP scaffolds, which prevented accurate measurement.

Microglial immunoreactivity

IBA-1-positive activated microglia were observed in all groups at 1 week and declined by 1 month (Fig. 2A), reflecting a decrease in microglial activation. Notably, there was significantly less activated microglia (Fig. 3A, $p < 0.05$) in the PCL-TCP group at week 1. By 1 month, all groups had approximately the same number of activated microglia. The intensity of *IBA-1*-positive microglia also decreased with increase in time, reflecting a decline in the level of inflammation.

GFAP *immunoreactivity*

A significant elevation in *GFAP* immunoreactivity was observed (Fig. 2B) at week 1 (Fig. 3B, $p < 0.05$). *GFAP* immunoreactivity was marked by a distribution of *GFAP*-positive astrocytes with hypertrophic soma and processes in the hippocampal area. In particular, measurement of the astrocyte area proximal to the TBI site confirmed hypertrophy, with a 75% increase in the astrocyte area in the control group, and ~55% increase in the astrocyte area in both the PCL and PCL-TCP groups (Fig. 3C, $p > 0.05$). By 1 month, *GFAP* immunoreactivity was greatly reduced, with the astrocyte area proximal to the TBI site measuring at the most 12.1% larger (PCL-TCP, $p > 0.05$) than astrocytes distal to the TBI site. *GFAP*-positive cells were observed in all groups at week 1 and declined by 1 month. The posthypertrophy astrocyte area measured from *GFAP* images revealed a significant decrease ($p < 0.05$) by 1 month among all groups, suggesting that astrocyte activation has declined (Fig. 3C). No significant differences were found among all groups at 1 month.

Nestin immunoreactivity

In all operated rat brains, nestin-positive cells with morphological characteristics similar to that of reactive astrocytes (hypertrophic soma and processes) were observed in the hippocampal area, proximal to the TBI site (Fig. 2D). By using ImageJ to calculate the level of brightness of the nestin stains belonging to the respective groups (where a lower level of brightness indicated a higher intensity of nestin staining), it was found that at week 1, PCL-TCP induced a significantly higher intensity of nestin stain (Fig. 3D, $p < 0.05$). Nestin immunoreactivity, a populated marker of neural progenitor cells, was intense at week 1 and had reduced in intensity by 1 month across all groups (Figs. 2D and 3D).

Neuronal damage—NeuN *and H&E staining*

NeuN-positive neuronal nuclei could be observed throughout the hippocampal region. Proximal to the TBI site (within 0.9 mm), neurons were shrunken and darkly stained (Fig. 2C). Similarly, H&E stains (Fig. 4) revealed a portion of neurons that were eosinophilic with pyknotic nuclei. Through observation, neuronal cells did not appear to infiltrate the area of insult regardless of control, PCL, or PCL-TCP groups.

By conducting a measurement of the cell nuclei size, it was found that at week 1 in the PCL-TCP scaffolds, the neurons proximal (within 0.9 mm) were 32.2% smaller (Table 1, $p < 0.05$) than those distal to the defect site (>1 mm). In the PCL group, the neuronal size was ~26.9% smaller (Table 1, $p < 0.05$). Between PCL-TCP and PCL scaffolds, the former has the smaller neuronal size (Table 1, $p < 0.05$). In the control group, neurons were found to be 33.3% smaller than in nondisturbed neurons (Table 1, $p < 0.05$).

Discussion

In this work, 70% porous PCL and PCL-TCP scaffolds were implanted into rat brains to primarily investigate the brain tissue inflammatory response to PCL-TCP scaffolds. While PCL has been shown to support regeneration in TBI,[6] no prior work has been conducted on the interaction of PCL-TCP porous scaffolds with brain tissue. Nonetheless, PCL-TCP scaffolds have been investigated for bone TE applications with reasonable success.[14,24,25]

Inflammatory responses at the edges of the scaffold could still be determined with *IBA-1*-expressing microglial, and *GFAP*-expressing hypertrophic astrocytes. *IBA-1* results

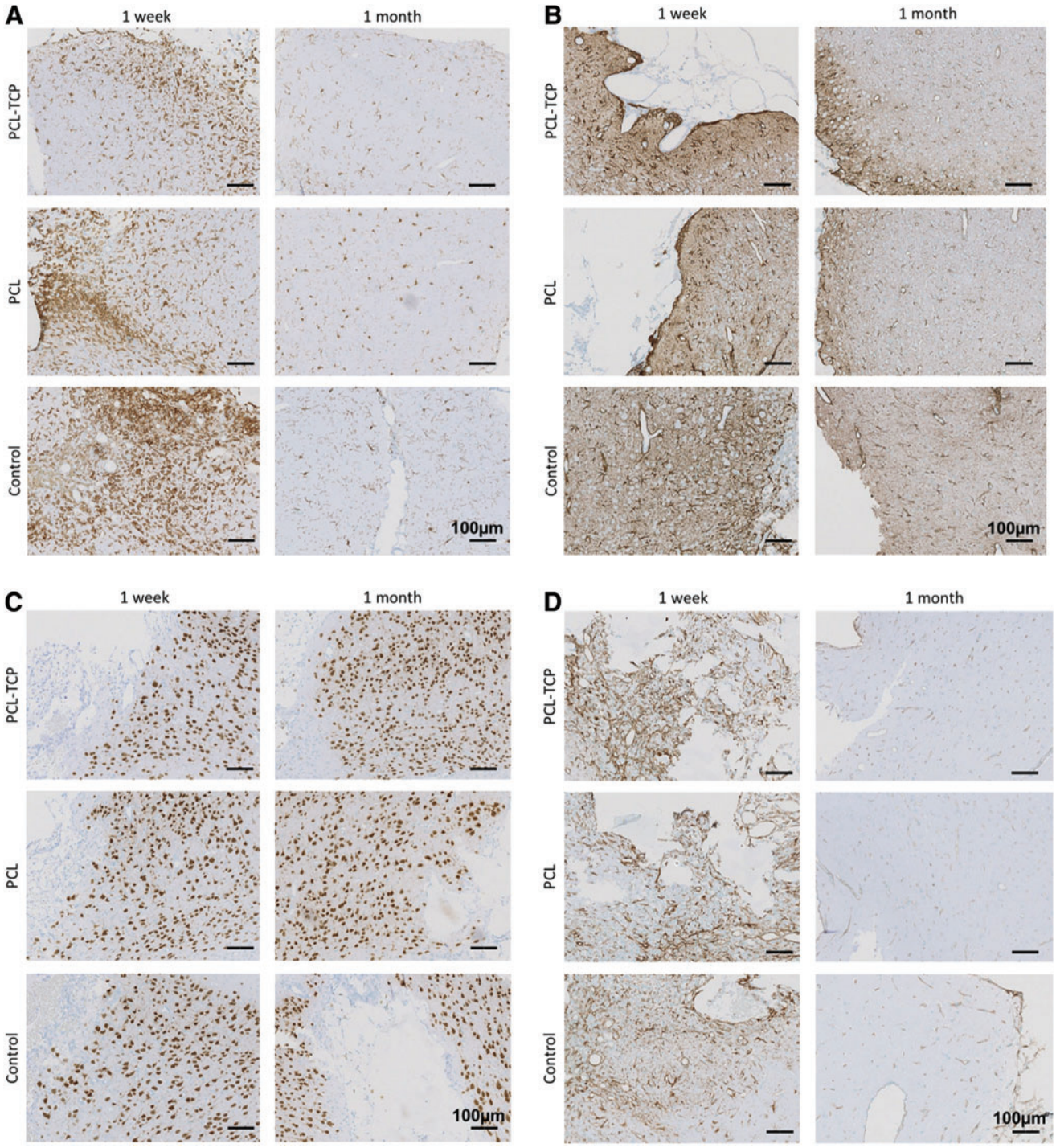

FIG. 2. Immunohistological staining for **(A)** microglial *(IBA-1)*, **(B)** astrocytes (*GFAP*), **(C)** neurons (*NeuN*), and **(D)** neurogenesis (nestin). **(A)** and **(B)** indicate that the levels of inflammation across all groups decreased over time. Observable difference in the intensity of staining for *IBA-1* **(A)** in the PCL-TCP scaffolds as compared to PCL was noted. Neuronal arrangement was disordered across all groups **(C)**. The neurogenic potential was not retained over time, with a down-regulation of nestin at 1 month **(D)**. Images were taken at 10×magnification. Scale bar represents 100 μm. PCL-TCP, polycaprolactone–tricalcium phosphate; *IBA-1*, ionized calcium binding adaptor molecule-1; *GFAP*, glial fibrillary acidic protein; *NeuN*, nestin and neuronal nuclei. Color images available online at www.liebertpub.com/tea

indicated that PCL-TCP scaffolds activated fewer microglial cells initially (Fig. 3A, $p<0.05$), suggesting that PCL-TCP elicits similar responses from the immune system as that of a defect without an implant. This suggests that PCL-TCP, as compared to PCL, attenuates the immune response. A possible reason for the attenuated response could lie in the degradation characteristics of PCL-TCP scaffolds. According to previous published results on the degradation of PCL[26] and PCL-TCP scaffolds,[23] the addition of TCP to the PCL matrix was reported to result in an increase in pH over

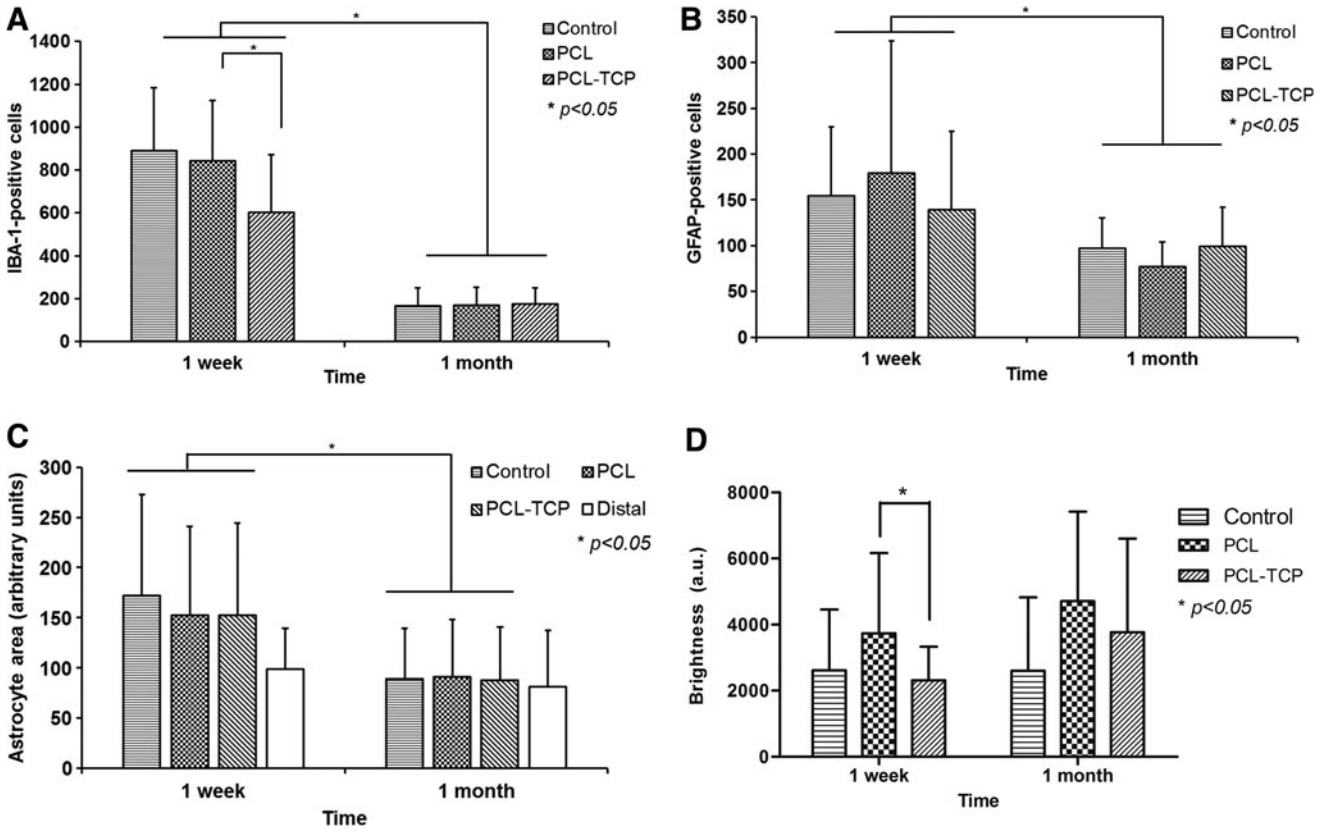

FIG. 3. Cellular count and area were measured at regions proximal to the defect site (within 0.9 mm of defect). **(A)** *IBA-1* activated microglial over time. There were significantly fewer inflammatory cells for the PCL-TCP group at 1 week ($p < 0.05$). Inflammation decreased to similar levels across all groups by 1 month. **(B)** Astrocyte activation was found to be similar across all groups at both 1 week and 1 month. **(C)** The astrocyte area was measured using ImageJ software following image processing. There were no significant differences among all groups at both 1 week and 1 month. The white bar represents the astrocyte area measured at distal regions from the defect site. **(D)** Nestin stain intensity quantified using ImageJ analysis. A higher intensity, as represented by lower brightness, was reported for PCL/TCP scaffolds as opposed to PCL ($p < 0.05$) on the first week. *$p < 0.05$. GFAP, glial fibrillary acidic protein.

time[23] due to the presence of TCP, which are alkaline in nature. The pH reached a level of ~8 by 4 weeks *in vitro*. Importantly, Lardner[27] reviewed the effect of pH on immune function, and has suggested that a slightly alkaline pH attenuates the immune response, while clinical acidosis is accompanied by impaired immunoefficiency. In view of the above, a locally elevated pH might have led to the lower activation of microglial cells in PCL-TCP scaffolds.

An earlier study by Wong *et al.*[6] reported that OX-42-positive activated microglia decreased over the duration of 4 weeks in the control and PCL groups, which was similar to our results. However, in terms of astrocyte activation, PCL sponges maintained astrocyte activation over time, while PCL scaffolds in our work reported a significant decline in *GFAP*-positive activated astrocytes, as did PCL-TCP scaffolds (Fig. 3B). This result, taken together with the lowered activation of *IBA-1* microglial, suggested that inflammation has decreased in our PCL and PCL-TCP scaffolds. Additionally, a drop in microglial levels over time without a corresponding decrease in astrocyte activation suggested that microglial activation might have mediated astrocytic activation, which subsequently affected the ability of astrocytes to form glial scars. This phenomenon was labeled as a time-dependent effect of activated microglia-related glial scar formation. In our work, a decrease in activated microglia over time (Fig. 3A) resulted in a corresponding decrease in activated astrocyte count and size (Fig. 3B, C) over time. Therefore, microglial activation did not appear to have a time-dependent effect on glial scar formation here. It was suggested by Streit[28] that microglial performs neuroprotective roles, but we believe that their roles have manifested in a different fashion. We observed that initial astrocyte activation in PCL and PCL-TCP scaffolds were comparable to control, while at the same time, microglial activation was significantly lower in the PCL-TCP scaffolds. Thus, it appears that the neuroprotective function that microglial has on astrocyte activation is more significant when a critical number of microglial cells are present.

It is known that following any injury or disease to the CNS, a typical reaction known as astrogliosis occurs. This reaction is characterized by hypertrophy and hyperplasia, in synchrony with the expression of the *GFAP* gene.[29] Astrocyte activation following TBI may be beneficial to damaged neurons by regulating neurotransmitter levels, repair of the ECM, control of blood-CNS interface, and transport processes, and trophic support to damaged cells. However, gliosis has also been suggested to interfere with residual neuronal circuits, negatively impacting the repair process, or

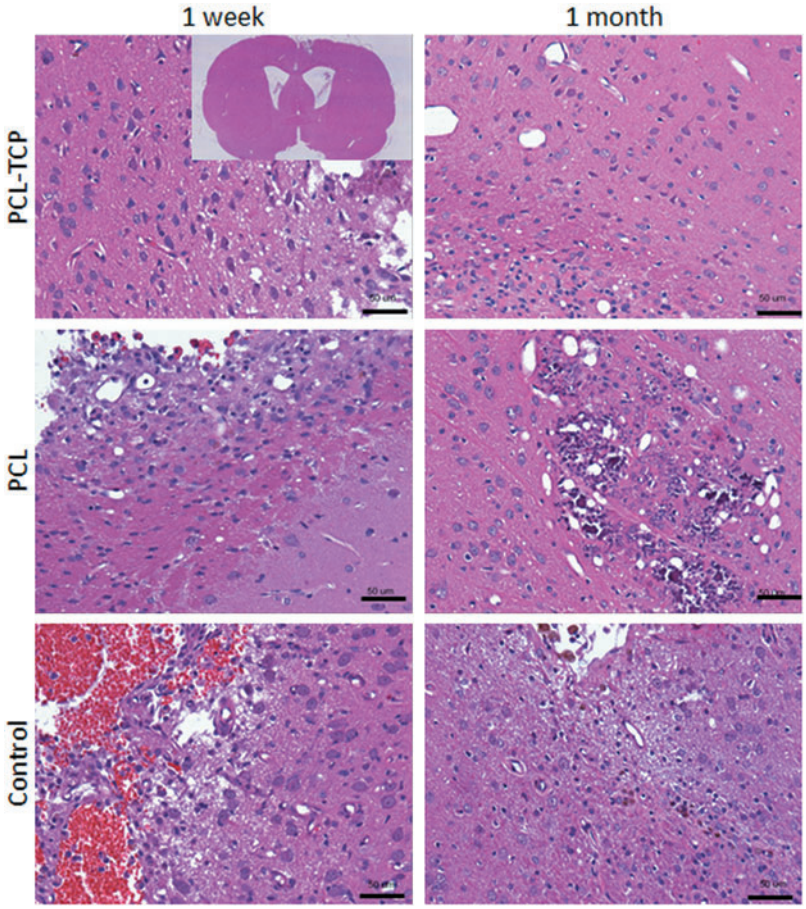

FIG. 4. Hematoxylin and eosin staining images, taken at 20× magnification. In all groups, eosinophilic neurons could be observed (darkly stained), indicating irreversible neuronal damage. A representative overview of the histological section has been shown in the inset. Scale bar represents 50 μm. Color images available online at www.liebertpub.com/tea

preventing remyelination. Despite this, reactive astrocytes and microglia regulate the migration and function of each other via the release of cytokines like interlukin-1 (IL-1) and tumor necrosis factor-alpha, which subsequently upregulates expression of IL-6 and transforming growth factor-beta, of which TGF-β has been shown to limit inflammation.[29,30]

The levels of astrocytes and microglia found in the parenchyma can serve as a gauge to the level of inflammation. In general, acute inflammation sets in within the first week, following which, chronic inflammation occurs.[31,32] As a result, differences in tissue responses would have begun in the first week, and become apparent by 1 month. The degradation of PCL-TCP scaffolds, both *in vitro* and *in vivo*, has been reported by our group.[23] Of interest to the current work, the *in vivo* degradation of PCL-TCP scaffolds implanted in rabbit abdomens was reported to result in a significant decrease in the molecular number (79.6%) and molecular weight (88.7%) over a period of 24 weeks. Despite the long degradation time, the mechanical properties of the PCL-TCP scaffolds could sufficiently match that of the cancellous bone, suggesting good scaffold mechanical integrity. Previous results investigating the degradation of PCL scaffolds suggested that they have a long degradation life of 2–4 years, depending on the initial molecular weight.[33,34] Based on the information above, PCL-TCP has a higher degradation rate than PCL, which could potentially lead to the formation of low molecular weight by-products (8000 g/mol).[23] This could potentially have resulted in higher macrophage activation, leading to phagocytosis of the degradation by-products. This phenomenon was, however, not observed. In fact, the levels of inflammation of PCL-TCP scaffolds were significantly lower (*IBA-1*-positive) initially as compared to PCL and control (Fig. 3A, $p < 0.05$). As mentioned earlier, the locally elevated pH could have mediated the inflammation response. Considering that acute inflammation has been significantly lowered, it reflects the advantage that PCL-TCP has over PCL scaffolds in terms of brain tissue inflammatory responses.

Table 1. Neuronal Size Differences Among the Various Groups

Implant	*Proximal (< 0.9 mm)*	*Distal (> 0.9 mm)*	*Decrease (%, proximal vs. distal)*
PCL	114 ± 47	156 ± 75	26.9[a]
PCL-TCP	106 ± 45	156 ± 75	32.2[a]
Control	110 ± 47	165 ± 76	33.3[a]

Significant decreases in neuronal nuclei size were recorded in all groups between proximal and distal regions after 1 week ([a]$p < 0.05$). Proximal to the defect site, PCL-TCP implants recorded a significantly smaller neuronal nuclei size as compared to PCL ([b]$p < 0.05$), and which was comparable to that of the control. The results are an average of 800 measurements over three images per implant group.

PCL-TCP, polycaprolactone–tricalcium phosphate.

Conclusion

From the presented data, brain tissue reaction to PCL and PCL-TCP scaffolds has been investigated by inflammatory response staining *(IBA-1)*, hypertrophy and hyperplasia of reactive astrocytes (*GFAP*). The effect of PCL and PCL-TCP scaffolds on neurogenic potential and neurons has also been investigated, and results have indicated that PCL and PCL-TCP do not evoke an undesirable inflammatory response, with notable advantage in PCL-TCP scaffolds. Additionally, neurogenic potential is not negatively impacted. In conclusion, results have suggested the brain tissue compatibility of PCL-TCP scaffolds.

Acknowledgments

This work was funded by the National University Health System Clinician's Research Grant. The authors would like to express their gratitude toward Mary Kan for her contribution to histopathology, Kian Chye for his involvement as a perfusionist, Dr. Enoka for her help in the IACUC application, and Dr. Yang Ming for helping out in the procedure.

Disclosure Statement

The authors declare that there is no conflict of interest involved in this work.

References

1. Johann, V., Schiefer, J., Sass, C., Mey, J., Brook, G., Krüttgen, A., Schlangen, C., Bernreuther, C., Schachner, M., Dihné, M., and Kosinski, C. Time of transplantation and cell preparation determine neural stem cell survival in a mouse model of Huntington's disease. Exp Brain Res **177,** 458, 2007.
2. Mahmood, A., Lu, D., and Chopp, M. Marrow stromal cell transplantation after traumatic brain injury promotes cellular proliferation within the brain. Neurosurgery **55,** 1185, 2004.
3. Xiong, Y., Lu, D., Qu, C., Goussev, A., Schallert, T., Mahmood, A., and Chopp, M. Effects of erythropoietin on reducing brain damage and improving functional outcome after traumatic brain injury in mice. J Neurosurg **109,** 510, 2008.
4. Mahmood, A., Lu, D., Qu, C., Goussev, A., and Chopp, M. Treatment of traumatic brain injury with a combination therapy of marrow stromal cells and atorvastatin in rats. Neurosurgery **60,** 546; discussion 53, 2007.
5. Yoshimura, S., Takagi, Y., Harada, J., Teramoto, T., Thomas, S.S., Waeber, C., Bakowska, J.C., Breakefield, X.O., and Moskowitz, M.A. FGF-2 regulation of neurogenesis in adult hippocampus after brain injury. Proc Natl Acad Sci U S A **98,** 5874, 2001.
6. Wong, D.Y., Hollister, S.J., Krebsbach, P.H., and Nosrat, C. Poly(epsilon-caprolactone) and poly (L-lactic-co-glycolic acid) degradable polymer sponges attenuate astrocyte response and lesion growth in acute traumatic brain injury. Tissue Eng **13,** 2515, 2007.
7. Mouriño, V., and Boccaccini, A.R. Bone tissue engineering therapeutics: controlled drug delivery in three-dimensional scaffolds. J R Soc Interface **7,** 209, 2010.
8. O'Keefe, R.J., and Mao, J. Bone tissue engineering and regeneration: from discovery to the clinic—an overview. Tissue Eng Part B Rev **17,** 389, 2011.
9. Tate, M.C., Shear, D.A., Hoffman, S.W., Stein, D.G., and LaPlaca, M.C. Biocompatibility of methylcellulose-based constructs designed for intracerebral gelation following experimental traumatic brain injury. Biomaterials **22,** 1113, 2001.
10. Wells, M.R., Kraus, K., Batter, D.K., Blunt, D.G., Weremowitz, J., Lynch, S.E., Antoniades, H.N., and Hansson, H.A. Gel matrix vehicles for growth factor application in nerve gap injuries repaired with tubes: a comparison of biomatrix, collagen, and methylcellulose. Exp Neurol **146,** 395, 1997.
11. Tian, W.M., Hou, S.P., Ma, J., Zhang, C.L., Xu, Q.Y., Lee, I.S., Li, H.D., Spector, M., and Cui, F.Z. Hyaluronic acid-poly-D-lysine-based three-dimensional hydrogel for traumatic brain injury. Tissue Eng **11,** 513, 2005.
12. Yasuda, H., Kuroda, S., Shichinohe, H., Kamei, S., Kawamura, R., and Iwasaki, Y. Effect of biodegradable fibrin scaffold on survival, migration, and differentiation of transplanted bone marrow stromal cells after cortical injury in rats. J Neurosurg **112,** 336, 2010.
13. Ng, K.W., Hutmacher, D.W., Schantz, J.T., Ng, C.S., Too, H.P., Lim, T.C., Phan, T.T., and Teoh, S.H. Evaluation of ultrathin poly(epsilon-caprolactone) films for tissue-engineered skin. Tissue Eng **7,** 441, 2001.
14. Rai, B., Ho, K.H., Lei, Y., Si-Hoe K-M, Jeremy Teo C-M, Yacob Kb, Chen, F., Ng, F.-C., and Teoh, S.H. Polycaprolactone-20% tricalcium phosphate scaffolds in combination with platelet-rich plasma for the treatment of critical-sized defects of the mandible: a pilot study. J Oral Maxillofac Surg **65,** 2195, 2007.
15. Yeo, A., Wong, W.J., Khoo, H.H., and Teoh, S.H. Surface modification of PCL-TCP scaffolds improve interfacial mechanical interlock and enhance early bone formation: an *in vitro* and *in vivo* characterization. J Biomed Mater Res Part A **92A,** 311, 2010.
16. Zhang, Z.Y., Teoh, S.H., Chong, M.S.K., Lee, E.S.M., Tan, L.G., Mattar, C.N., Fisk, N.M., Choolani, M., and Chan, J. Neo-vascularization and bone formation mediated by fetal mesenchymal stem cell tissue-engineered bone grafts in critical-size femoral defects. Biomaterials **31,** 608, 2010.
17. Rai, B., Teoh, S.H., Hutmacher, D.W., Cao, T., and Ho, K.H. Novel PCL-based honeycomb scaffolds as drug delivery systems for rhBMP-2. Biomaterials **26,** 3739, 2005.
18. Teo, E.Y., Ong, S.-Y., Khoon Chong, M.S., Zhang, Z., Lu, J., Moochhala, S., Ho, B., and Teoh, S.-H. Polycaprolactone-based fused deposition modeled mesh for delivery of antibacterial agents to infected wounds. Biomaterials **32,** 279, 2011.
19. Dietmar, W.H. Scaffolds in tissue engineering bone and cartilage. Biomaterials **21,** 2529, 2000.
20. Zein, I., Hutmacher, D.W., Tan, K.C., and Teoh, S.H. Fused deposition modeling of novel scaffold architectures for tissue engineering applications. Biomaterials **23,** 1169, 2002.
21. Hutmacher, D.W., Schantz, T., Zein, I., Ng, K.W., Teoh, S.H., and Tan, K.C. Mechanical properties and cell cultural response of polycaprolactone scaffolds designed and fabricated via fused deposition modeling. J Biomed Mater Res **55,** 203, 2001.
22. Schantz, J.-T., Brandwood, A., Hutmacher, D., Khor, H., and Bittner, K. Osteogenic differentiation of mesenchymal progenitor cells in computer designed fibrin-polymer-ceramic scaffolds manufactured by fused deposition modeling. J Mater Sci Mater Med **16,** 807, 2005.

23. Yeo, A., Rai, B., Sju, E., Cheong, J.J., and Teoh, S.H. The degradation profile of novel, bioresorbable PCL–TCP scaffolds: An *in vitro* and *in vivo* study. J Biomed Mater Res Part A **84A,** 208, 2008.
24. Lim, H.C., Bae, J.H., Song, H.R., Teoh, S.H., Kim, H.K., and Kum, D.H. High tibial osteotomy using polycaprolactone-tricalcium phosphate polymer wedge in a micro pig model. J Bone Joint Surg Br Vol **93B,** 120, 2011.
25. Rai, B., Oest, M.E., Dupont, K.M., Ho, K.H., Teoh, S.H., and Guldberg, R.E. Combination of platelet-rich plasma with polycaprolactone-tricalcium phosphate scaffolds for segmental bone defect repair. J Biomed Mater Res Part A **81A,** 888, 2007.
26. Sun, H., Mei, L., Song, C., Cui, X., and Wang, P. The *in vivo* degradation, absorption and excretion of PCL-based implant. Biomaterials **27,** 1735, 2006.
27. Lardner, A. The effects of extracellular pH on immune function. J Leukoc Biol **69,** 522, 2001.
28. Streit, W.J. Microglia as neuroprotective, immunocompetent cells of the CNS. Glia **40,** 133, 2002.
29. Ghirnikar, R.S., Lee, Y.L., and Eng, L.F. Inflammation in traumatic brain injury: role of cytokines and chemokines. Neurochem Res **23,** 329, 1998.
30. Logan, A., and Berry, M. Transforming growth factor-β1 and basic fibroblast growth factor in the injured CNS. Trends Pharmacol Sci **14,** 337, 1993.
31. Bramlett, H.M., and Dietrich, W.D. Pathophysiology of cerebral ischemia and brain trauma[colon] Similarities and differences. J Cereb Blood Flow Metab **24,** 133, 2004.
32. Williams, A.J., Hartings, J.A., Lu, X.C., Rolli, M.L., and Tortella, F.C. Penetrating ballistic-like brain injury in the rat: differential time courses of hemorrhage, cell death, inflammation, and remote degeneration. J Neurotrauma **23,** 1828, 2006.
33. Middleton, J.C., and Tipton, A.J. Synthetic biodegradable polymers as orthopedic devices. Biomaterials **21,** 2335, 2000.
34. Gunatillake, P.A., and Adhikari, R. Biodegradable synthetic polymers for tissue engineering. Eur Cell Mater **5,** 1; discussion, 2003.

Address correspondence to:
Swee-Hin Teoh, PhD
Division of Bioengineering
School of Chemical and Biomedical Engineering
Nanyang Technological University
70 Nanyang Drive, N1.3
Singapore 637457
Singapore

E-mail: teohsh@ntu.edu.sg

Received: December 10, 2012
Accepted: May 5, 2013
Online Publication Date: July 25, 2013